ACS APPLIED MATERIALS & INTERFACES

Research Article

Cite This: ACS Appl. Mater. Interfaces 2018, 10, 5793−5804

www.acsami.org

Water on Graphene-Coated TiO_2: Role of Atomic Vacancies

Martina Datteo, Hongsheng Liu, and Cristiana Di Valentin*

Dipartimento di Scienza dei Materiali, Università di Milano-Bicocca, via R. Cozzi 55, I-20125 Milano, Italy

Supporting Information

ABSTRACT: Beyond two-dimensional (2D) materials, interfaces between 2D materials and underlying supports or 2D-coated metal or metal oxide nanoparticles exhibit excellent properties and promising applications. The hybrid interface between graphene and anatase TiO_2 shows great importance in photocatalytic, catalytic, and nanomedical applications due to the excellent and complementary properties of the two materials. Water, as a ubiquitous and essential element in practical conditions and in the human body, plays a significant role in the applications of graphene/TiO_2 composites for both electronic devices and nanomedicine. Carbon vacancies, as common defects in chemically prepared graphene, also need to be considered for the application of graphene-based materials. Therefore, the behavior of water on top and at the interface of defective graphene on anatase TiO_2 surface was systematically investigated by dispersion-corrected hybrid density functional calculations. The presence of the substrate only slightly enhances the on-top adsorption and reduces the on-top dissociation of water on defective graphene. However, at the interface, dissociated water is largely preferred compared with undissociated water on bare TiO_2 surface, showing a prominent cover effect. Reduced TiO_2 may further induce oxygen diffusion into the bulk. Our results are helpful to understand how the presence of water in the surrounding environment affects structural and electronic properties of the graphene/TiO_2 interface and thus its application in photocatalysis, electronic devices, and nanomedicine.

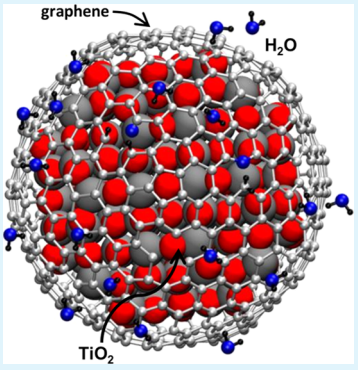

KEYWORDS: *graphene/TiO_2 interface, carbon vacancy, oxygen vacancy, water reactivity, hydrophilicity, catalysis under cover*

1. INTRODUCTION

Graphene, as the prototype of two-dimensional (2D) materials, shows excellent properties and has been widely studied.[1−3] Moreover, graphene can anchor or wrap metal and metal oxide nanoparticles effectively to form various nanocomposites, which show great potential in catalytic applications.[4−7] Among these nanocomposites, TiO_2−graphene nanocomposites have drawn great attention because TiO_2 possesses superior photocatalytic performance, good biocompatibility, and chemical and thermal stabilities.[8−10] In recent years, graphene-coated TiO_2 nanoparticles have also been synthesized in experiments and found to show enhanced photocatalytic activity.[11−14] The observed improved performance in photocatalysis and photovoltaics of TiO_2−graphene nanocomposites is attributed to the presence of the graphene layer.[8−10] On one hand, graphene can act as an electron acceptor to effectively hinder the electron−hole pair recombination upon UV irradiation of TiO_2;[8,9,11,15−18] on the other, if TiO_2−graphene nanocomposites are exposed to visible light, graphene can act as sensitizer with electrons being photoexcited within the graphene states and then eventually trapped by Ti atoms, after direct transfer to the TiO_2 conduction band.[10,19,20] Moreover, graphene-coated TiO_2 nanoparticles exhibit great applications in lithium-ion batteries,[21−23] in biosensors,[24] and are also rather promising in the field of nanomedicine because graphene and TiO_2 have a good performance for carrying bioactive molecules[25] and for photodynamic therapy,[26] respectively.

In real TiO_2−graphene nanocomposite samples, graphene is expected to present defects[27] that may play an important role. Carbon vacancies can naturally form during the growth process. Eventually, they could be also generated on purpose through particle irradiations or chemical treatments.[28] For example, one widely used approach to prepare graphene-based/TiO_2 composite photocatalysts is the reduction of graphene oxide (GO).[29] This GO-derived graphene inevitably contains few residual amounts of oxygenated functional groups and a particularly large population of defects. Another very common approach to obtain graphene−TiO_2 composite is to use graphite dispersion and exfoliation,[30,31] which also leads to defective graphene samples that present carbon vacancies, as experimentally observed by TEM.[32,33] Defects do not always appear as unfavorable factors, reducing or even degrading the excellent qualities of graphene. They can also be used, exploited, and even properly designed to suite desirable purposes. For instance, vacancies in graphene sheets or nanotubes can be used as traps for metal atoms, by providing strong C−metal bonds.[34,35] Vacancies are good anchoring points for deposition of nanoparticles[34,36−38] and can enhance the catalytic activity of the nanoparticles. The CO oxidation barrier[36] and O_2 dissociation activation energy[37] on small platinum nanoparticles are reduced when the platinum nanoparticles are supported on defective graphene. Moreover, defective graphene is also promising in the fields of hydrogen storage[39,40] and air purification.[41] Recent theoretical study

Received: November 28, 2017
Accepted: January 25, 2018
Published: January 25, 2018

DOI: 10.1021/acsami.7b18087
ACS Appl. Mater. Interfaces 2018, 10, 5793−5804

shows that vacancy defects can highly enhance the binding between graphene and metal surfaces (Cu and Pt) by forming strong organometallic bonds.[42] Therefore, defects may have a big influence on the graphene/TiO_2 interface and thus affect the performance of TiO_2−graphene nanocomposites.

Water is ubiquitous in normal environmental conditions and especially in human bodies. Thus, the behavior of water at the interface of graphene-coated TiO_2 (i.e., G/TiO_2) is of great interest and significance for the applications of TiO_2−graphene nanocomposites in photocatalysis, lithium-ion batteries, biosensors, and nanomedicine. Recently, the reactivity of water molecules on top and at the interface of nondefective G/TiO_2 composite was studied by density functional theory (DFT) calculations.[43] On top of G/TiO_2, water physically adsorbs on the graphene layer with an adhesion energy slightly larger than that on freestanding graphene. At the interface, H_2O prefers to adsorb on TiO_2 rather than on the carbon sheet, leading to adsorption configurations very similar to those on bare TiO_2. Thus, the appearance of graphene does not improve the activity for water dissociation. However, the presence of carbon vacancies in the graphene layer may rather affect the situation but it is still an open question.

Many exciting results have been recently achieved, exploiting the confined space between graphene or other 2D materials and an underlying support for different reactions of small molecules, like H_2, O_2, CO, and H_2O. For example, intercalated CO at the graphene/Pt(111) interface shows weaker interactions with the metal as well as lower desorption temperatures and a lower reaction barrier for oxidation compared to those of bare Pt(111).[5,44−46] The desorption of H_2 on Pt(111) surface is facilitated in the presence of either graphene or h-BN monolayer due to the cover effect.[47] Recent experiments show that oxygen can reach the graphene/Cu interface and lead to a partial oxidation of Cu.[48,49] In contrast, dissociation of O_2 at boron-doped graphene/Cu(111) interface leads to the competitive oxidation of the graphene sheet in the proximity of the dopant.[50] It is shown that water can reach the interface between graphene and different substrates, such as HfO_2,[51] silica,[52] $BaTiO_3$,[53] or Ni(111) surfaces,[54] by intercalation. Water intercalation under the epitaxial graphene on Ru(0001) surface can efficiently split the graphene along line defects into numerous fragments at temperatures as low as 90 K.[55] On Cu(111), however, the water-induced splitting of graphene is far less effective.[55] At the interface of graphene, with carbon vacancies on Cu(111) surface, water is capable of breaking the C−Cu bond by dissociating at the undercoordinated carbon atom of the vacancy, restoring the weak van der Waals type of interaction at the interface.[42] The same is not true in the case of Pt(111) surface, where C−Pt bonds are much stronger. Recent DFT calculations show that graphene-on-Cu is a good catalyst for water splitting and is suitable for the low-temperature process.[56] By X-ray absorption spectra, Böttcher and coworkers proposed that on Ni(111)-supported graphene,[57] water is not just physisorbed as on freestanding graphene[58] but it is chemically bound, inducing a p-type doping.[59] Moreover, water is expected to dissociate within the graphene/Ni(111) interface at room temperature, providing a hydrogenated graphene sheet with a gravimetric density competitive with current technology for hydrogen storage.[54]

In this work, by means of dispersion-corrected hybrid density functional theory (DFT) calculations, we investigate two atomic defects in the hybrid interface: C monovacancy in graphene and O vacancy in TiO_2. The C monovacancy can be considered a prototype defect in graphene because the undercoordinated C atoms appearing in the structure are analogous to those that would appear in the presence of larger (pluriatomic) vacancies or in the presence of extended edges. The O vacancy is a prototype defect for reduced TiO_2 samples, which are those commonly obtained after annealing. First, we study the structural and electronic properties of the interface between graphene with one C monovacancy (VG) and the stoichiometric anatase TiO_2(101) surface (VG/TiO_2). Then, we analyze the behavior of water at the interface. Finally, we consider the effect of the presence of one O vacancy in the TiO_2 support. Our results show that the characteristic magnetism of freestanding VG[60] quenches in the presence of an underlying anatase TiO_2(101) surface and a C−O bond may occur at the interface. Dissociated rather than molecular water is preferred at the interface VG/TiO_2 in contrast with what is observed on bare TiO_2 surface. O atoms at the interface may diffuse into the reduced TiO_2 sublayers to heal O vacancies. This study is helpful to understand how the presence of water in the surrounding environment affects structural and electronic properties of the graphene/TiO_2 interface and thus its application in photocatalysis, electronic devices, and nanomedicine.

2. COMPUTATIONAL METHODS

All of the calculations were performed with the CRYSTAL14 code,[61] where Kohn−Sham orbitals are expanded in Gaussian type functions (the all-electron basis sets are O 8-411(d1), Ti 86-411(d41), C 6-31(d1), and H-11(p1)). The hybrid functional B3LYP[62,63] was adopted for all of the calculations. To properly take into account the long-range van der Waals interactions, dispersion correction was introduced with the Grimme approach.[64,65] The lattice parameters of anatase were calculated to be 3.764 and 9.793 Å for *a* and *c*, respectively. The anatase (101) TiO_2 surface was modeled by a three triatomic layers slab (144 atoms), with the bottom layer fixed. A (5 × 6) supercell for graphene and a (4 × 2) supercell for anatase (101) slab were used to build the co-periodic lattice of the graphene/anatase (101) hybrid system. An angle of 50° exists between the vectors of the supercells of graphene and anatase (101) TiO_2 surface. Here, the lattice of graphene was slightly stretched in *x* direction and compressed in *y* direction (see Figure 1) to fit the anatase lattice. Thus, a slightly tensile strain along *x* axis (+1.9%) and compressive strain along *y* axis (−0.6%) were introduced. Therefore, two configurations appear for freestanding graphene with monovacancy,

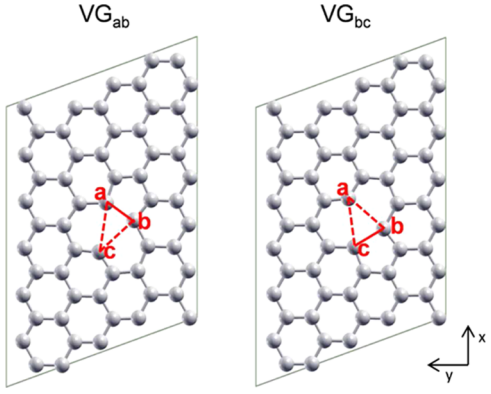

Figure 1. Two ball-and-stick configurations of slightly strained freestanding graphene with a single C vacancy: VG_{ab} and VG_{bc}. The red triangles indicate the vacancy defect. The solid red lines represent elongated C−C bonds and the dotted lines indicate no C−C bond. The three C atoms at the vacancy are marked a, b, and c.

DOI: 10.1021/acsami.7b18087
ACS Appl. Mater. Interfaces 2018, 10, 5793−5804

VG_{ab} and VG_{bc}, depending on the rearrangement of carbon atoms at the vacancy site, as shown in Figure 1. One carbon single vacancy was created in one supercell of VG/TiO_2, resulting in a distance larger than 11 Å between two periodically repeated defects and in a vacancy concentration of 1.67%. The difference between VG_{ab} and VG_{bc} is just the vacancy pattern when we repeat the supercell, as can be seen in Figure S1 in the Supporting Information (SI). VG_{bc} is 0.21 eV higher in energy than VG_{ab}. Thus, for the VG/TiO_2 interface, only VG_{ab} is presented in the manuscript. To make sure that we always get the reasonable VG/TiO_2 interface, VG_{bc}/TiO_2 interfaces were also calculated and are shown in Figure S2 in the SI, which are always higher in energy compared with VG_{ab}/TiO_2 interfaces.

The geometry optimizations were done using a 2 × 2 × 1 *k*-point mesh. A dense *k*-point mesh of 15 × 15 × 1 was adopted in the calculations for density of state (DOS) to get a good description of the electronic properties.

The adhesion energy of the interface VG/TiO_2 is defined as

$$\Delta E_{adh} = E(VG/TiO_2) - [E(VG) + E(TiO_2)] \quad (1)$$

where $E(VG/TiO_2)$ is the energy of the VG/TiO_2 interface, $E(VG)$ is the energy of freestanding VG, and $E(TiO_2)$ is the energy of the TiO_2 slab.

The adsorption energy (ΔE_{ads}) and dissociation energy (ΔE_{diss}) of water on freestanding VG are computed as follows

$$\Delta E_{ads\ or\ diss} = E(VG + H_2O) - [E(VG) + E(H_2O)] \quad (2)$$

where $E(VG + H_2O)$ is the total energy of molecular or dissociated H_2O on VG, $E(VG)$ is the energy of freestanding VG, and $E(H_2O)$ is the energy of an isolated H_2O molecule.

The same quantities (ΔE_{ads} and ΔE_{diss}) for water on bare $TiO_2(101)$ surface are computed as follows

$$\Delta E_{ads\ or\ diss} = E(TiO_2 + H_2O) - [E(TiO_2) + E(H_2O)] \quad (3)$$

where $E(TiO_2 + H_2O)$ is the total energy of molecular or dissociated H_2O on TiO_2 surface, $E(TiO_2)$ is the energy of the TiO_2 slab, and $E(H_2O)$ is the energy of an isolated H_2O molecule.

The same quantities (ΔE_{ads} and ΔE_{diss}) for water on top or at the interface of VG/TiO_2 are computed as follows

$$\Delta E_{ads\ or\ diss} = E(VG/TiO_2 + H_2O) - [E(VG/TiO_2) + E(H_2O)] \quad (4)$$

where $E(VG/TiO_2 + H_2O)$ is the total energy of molecular or dissociated H_2O on top or at the interface of VG/TiO_2, $E(VG/TiO_2)$ is the energy of the most stable configuration of the interface VG/TiO_2, and $E(H_2O)$ is the energy of an isolated H_2O molecule.

In the following, we define the nomenclature that will be used in the manuscript. We name the hybrid interface between graphene and the anatase $TiO_2(101)$ surface as "G/TiO_2" (Section 3.1). In the presence of one C monovacancy in G/TiO_2, we may observe interaction of the vacancy either with a 2-fold coordinated bridging oxygen (O_{br}) or a 5-fold coordinated Ti atom (Ti_{5c}) on the anatase $TiO_2(101)$ surface. If the type of interaction is a C−O covalent bond at the interface, we represent it by the symbol "—" ($VG—O_{br}$); if it is a weak van der Waals interaction, we represent it by the symbol "---" ($VG---O_{br}$ or $VG---Ti_{5c}$).

For the configurations of molecular water adsorption on VG/TiO_2 (Section 3.2.1), we use the symbol "/" when on top ($H_2O/VG—O_{br}$) and a second "/" when between the two materials ($VG/H_2O/TiO_2$).

For the configurations of dissociated water (in OH + H or O + H + H), further details must be given (Section 3.2.2). When on freestanding defective graphene, we add subscripts a, b, or c to each fragment of dissociation (e.g., OH_aH_b, $O_aH_bH_c$, or $O_{ab}2H_c$) that identify which uncoordinated C atoms at the vacancy site are involved in the bonding (see Figure 1 (left) or Figure 2 for the definition of C atoms a, b, and c). When the dissociation takes place on top or at the interface of VG/TiO_2, we do not explicitly mention VG/TiO_2 in the label but we use the generalized label ".../.../..." where the first "/" distinguishes what is on VG from what is at the interface and the second "/" distinguishes what is at the interface from what is on TiO_2:

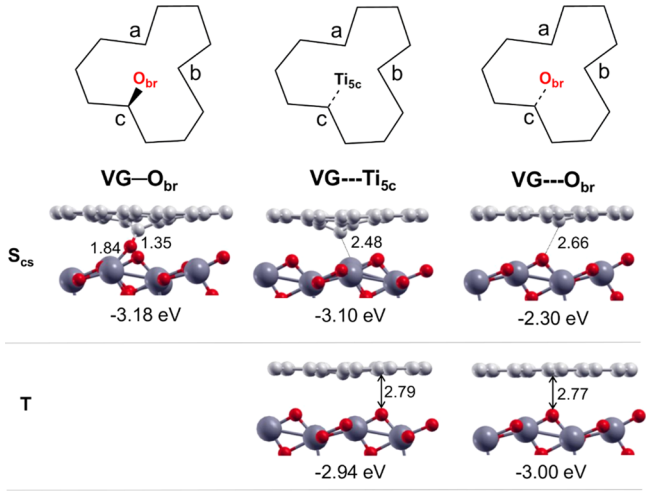

Figure 2. Schematic top views of the C monovacancy defect in VG/TiO_2 interfaces (top line). Side views of selected configurations of VG/TiO_2 interfaces in the singlet close shell (S_{cs}) (middle line) and in the triplet (T) solutions (bottom line). For labels, see Section 2 and Figure 1. Adhesion energies per supercell calculated according to eq 1 are listed below each configuration. Small red and light gray balls represent O atoms and C atoms. Big dark gray balls represent Ti atoms. Distances are in Å.

the fragments of dissociation bound to VG go on the left part of the label (e.g., OH_a/.../...), the fragments at the interface between VG and TiO_2 go in the central part of the label (e.g., .../OH_a/...), and the fragments on TiO_2 go on the right part of the label (e.g., .../.../$O_{br}H$ or .../.../$Ti_{5c}OH$), where O_{br} is a 2-fold coordinated O and Ti_{5c} is a 5-fold coordinated Ti on the anatase $TiO_2(101)$ surface. Accordingly, dissociated water on bare TiO_2 surface was simply labeled as "$Ti_{5c}OHO_{br}H$" (Section 3.2.3).

3. RESULTS AND DISCUSSION

3.1. Interface between Defective Graphene and $TiO_2(101)$ Surface. The ground state for VG is calculated to be triplet with a planar configuration, which is in accordance with a previous study.[60] After the formation of one single vacancy in the graphene sheet, there is a dangling bond on the C_c atom with a sp^2 hybridization, whereas the other two carbon atoms (a and b) get closer to form an elongated C−C bond (labeled as VG_{ab} in Figure 1). The singlet close shell solution for VG with a buckled high of 0.62 Å at the vacancy was found to be 0.50 eV higher in energy than the corresponding triplet solution. However, considering that the magnetism may quench in the presence of $TiO_2(101)$ surface, both triplet and singlet close shell solutions were considered for the VG/TiO_2 interface.

Various different configurations of the VG/TiO_2 interfaces have been considered to search for the most stable one, including different relative positions between graphene and TiO_2 surface, as well as the mirror flipping of graphene. Some selective configurations of VG/TiO_2 interfaces are listed in Figure 2. Less stable configurations resulting from a mirror flipping of graphene are shown in Figure S3 in the SI. First, we focus on the singlet close shell structures.

When the VG was put close to the TiO_2 surface and above one bridge oxygen atom, the most stable interface $VG—O_{br}$ could be obtained after geometry optimization, with an adhesion energy of −3.18 eV per supercell. The ground state of this configuration is singlet close shell state, in which the carbon atom c (marked in Figure 2) is oxidized and forms a

DOI: 10.1021/acsami.7b18087
ACS Appl. Mater. Interfaces 2018, 10, 5793−5804

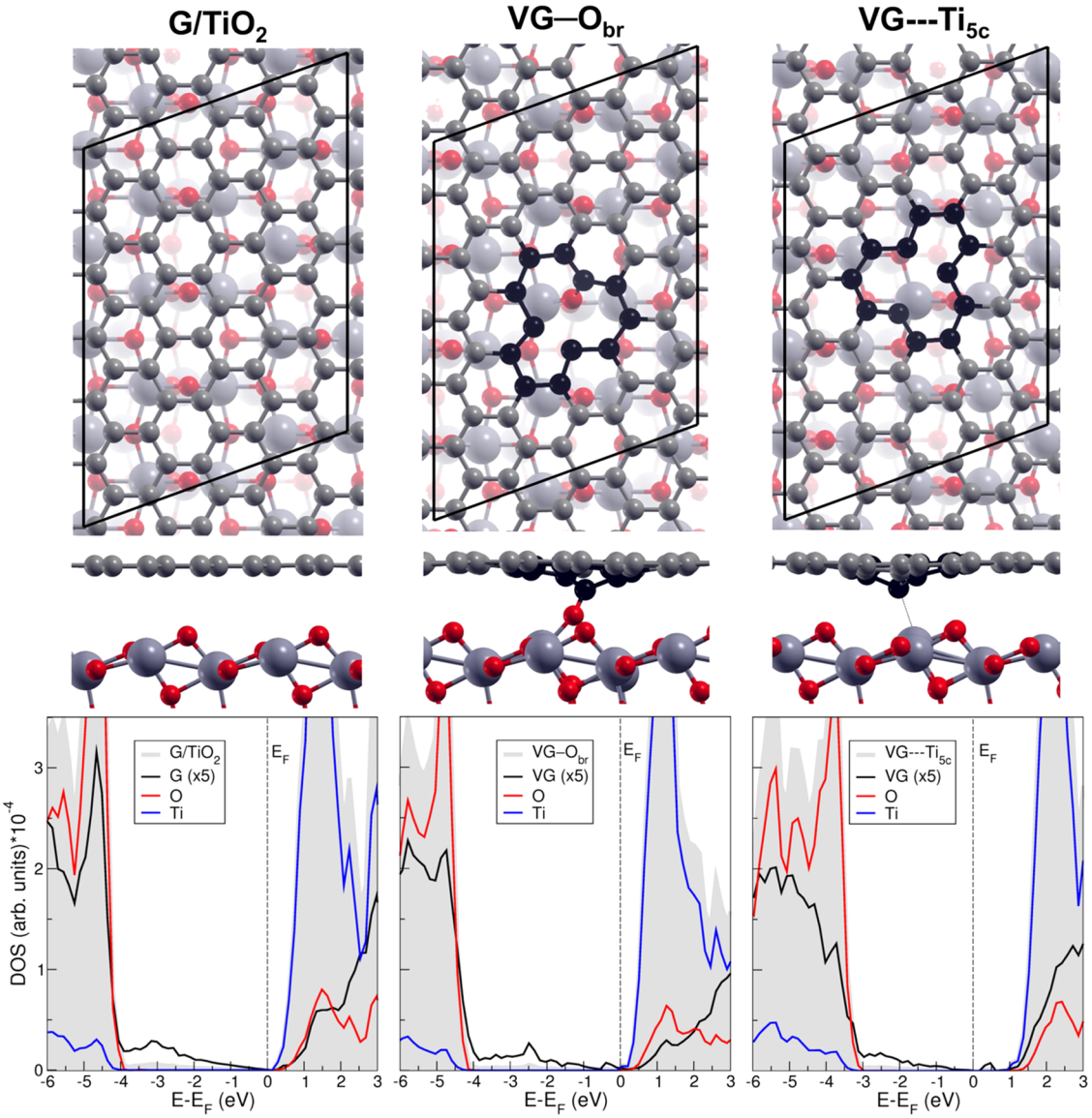

Figure 3. Top and side views of G/TiO_2, VG—O_{br}, and VG---Ti_{5c} interfaces (top and middle lines) along with the density of states (bottom line). The C atoms at the vacancy are highlighted in black, and the other C atoms are shown in light gray. Small red balls represent O atoms, and big dark gray balls represent Ti atoms. In the DOS, the filled gray area represents the total DOS and the black line is DOS-projected on graphene (G or VG), which is ×5 for clarity. The red and blue lines are DOS-projected on all O and all Ti atoms in the TiO_2 slab, respectively. Fermi energy (E_F) is set at the eigenvalue of the highest occupied states.

strong covalent bond with the O_{br} atom. The C−O bond length at the interface is 1.35 Å. One of the original two O−Ti bonds is broken, and the other one is elongated from 1.82 to 1.84 Å. This C−O−Ti bond agrees well with X-ray photoelectron spectra and Fourier transform infrared spectra of TiO_2/graphene nanocomposites in previous experiments.[66−68] This additional chemical bond between graphene and TiO_2, which is otherwise just attracted by dispersion forces, is crucial because it was shown to facilitate the interfacial charge transfer, improving the photocatalytic activity of TiO_2−graphene composites.[15,69]

Another metastable singlet configuration is the VG---Ti_{5c}, which is 80 meV higher in energy than VG—O_{br}. For VG---Ti_{5c}, in which the vacancy is above one 5-fold Ti atom on the TiO_2 surface, the carbon atom c moves down toward the Ti_{5c} atom to establish an interaction. However, the C−Ti distance is as long as 2.48 Å, much larger than the normal C−Ti bond length in C−Ti alloy (2.11−2.16 Å), implying that there is no true chemical bond at the interface. Actually, we never succeed in getting a C−Ti bond at the interface even when starting from a very short interface distance, which is in agreement with previous theoretical results about TiO_2 nanostructures on graphene.[70] Only for very small $(TiO_2)_n$ clusters ($n \leq 15$) on VG, some Ti−C bonds have been reported in the literature.[71] Another less stable singlet-state configuration for the interface is named as VG---O_{br}, in which the carbon atom c moved down toward one O_{br}. However, the C−O distance is very high (2.66 Å). Thus, there is no true chemical bond in this configuration at the interface and the adhesion energy is much smaller when compared to that of VG—O_{br}.

Now, we turn to the triplet solutions. The most stable two triplet configurations are shown in Figure 2. We observe that the triplet solutions for VG/TiO_2 are always characterized by the planar geometry of VG on TiO_2 surface, with an

DOI: 10.1021/acsami.7b18087
ACS Appl. Mater. Interfaces 2018, 10, 5793−5804

equilibrium distance between graphene and TiO_2 surface of about 2.8 Å, indicating weak van der Waals interactions at the interfaces. The adhesion energies at the interfaces are −2.94 and −3.00 eV per supercell for VG---Ti_{5c} and VG---O_{br}, respectively.

On the basis of the results above, we conclude that the magnetism of VG is quenched when it is supported on a TiO_2(101) surface because the singlet-state configurations for VG—O_{br} and for VG---Ti_{5c} are the most stable ones. The chemical adsorption of VG on TiO_2(101) (VG—O_{br}) involves the breaking of one O−Ti bond. Thus, we expect an energy barrier between physical and chemical adsorption. We suppose that after the transfer of graphene from the substrate for growth (for example Cu or Ni) to the TiO_2 anatase (101) surface, the interface presents a mixture of VG—O_{br} and VG---Ti_{5c}. So, hereafter, we will focus our work on these two most stable singlet close shell configurations.

The top and side views of G/TiO_2, VG—O_{br}, and VG---Ti_{5c} interface models are shown in Figure 3, where the relative position of the vacancy on the TiO_2 surface is clearly displayed. To further investigate and understand their electronic properties, the projected density of states is plotted under each structure. In all three systems, we observe that the C 2p states largely fill the TiO_2 band gap region. This can explain the broad background absorption in the visible-light region of TiO_2−graphene nanocomposites.[66,72] For the nondefective G/TiO_2 interface, the Dirac cone at the Fermi level originating from freestanding graphene is quite preserved and the total density of states is almost the superimposition of those from freestanding graphene and from TiO_2 surface due to the weak interaction at the interface, even though a small band gap opening is registered (0.14 eV).[19] We wish to recall, from a previous work by us,[60] that a small band gap opens also when the C monovacancy is introduced in the freestanding graphene (VG). This is 0.26 eV with the computational setup and supercell model used in the present work. It is very interesting to observe what happens when VG is now put on TiO_2. In the case of VG—O_{br} interface, the DOS presents some states originating from Ti atoms at the Fermi level; thus, there is no band gap but a metallic character is exhibited. This is a consequence of the Ti−O bond breaking at the TiO_2 surface that results in a non-fully oxidized TiO_2 surface. The metallic character of VG—O_{br} interface can be more clearly noted in the zoomed DOS shown in Figure 4a. On the contrary, for the VG---Ti_{5c} interface, a band gap of 0.27 eV is observed (see Figure 4b) due to the presence of the C vacancy, in line with the case of freestanding VG.[60]

To gain more insight on the interaction at the interfaces of VG—O_{br} and VG---Ti_{5c}, the projected density of states on C_c, O_{br}, and Ti_{5c} atoms are calculated and shown in Figure 4a,b, respectively. For VG—O_{br} interface, a clear hybridization between C_c p and O_{br} p orbitals exists in the energy range between −4 and −9.5 eV below the Fermi level due to the C−O chemical bond at the interface. For VG---Ti_{5c}, some hybridization between C_c p and Ti_{5c} d orbital can be seen in the energy range between −3 and −8 eV, in line with a strong interaction at the interface.

3.2. Reactivity with Water. In this section, we describe the water reactivity with the VG/TiO_2 interface in terms of molecular (Section 3.2.1) and dissociated (Section 3.2.2) adsorption modes. We consider the possibility that either water molecules approach from the top of the interface or they are intercalated through graphene edges or large carbon holes

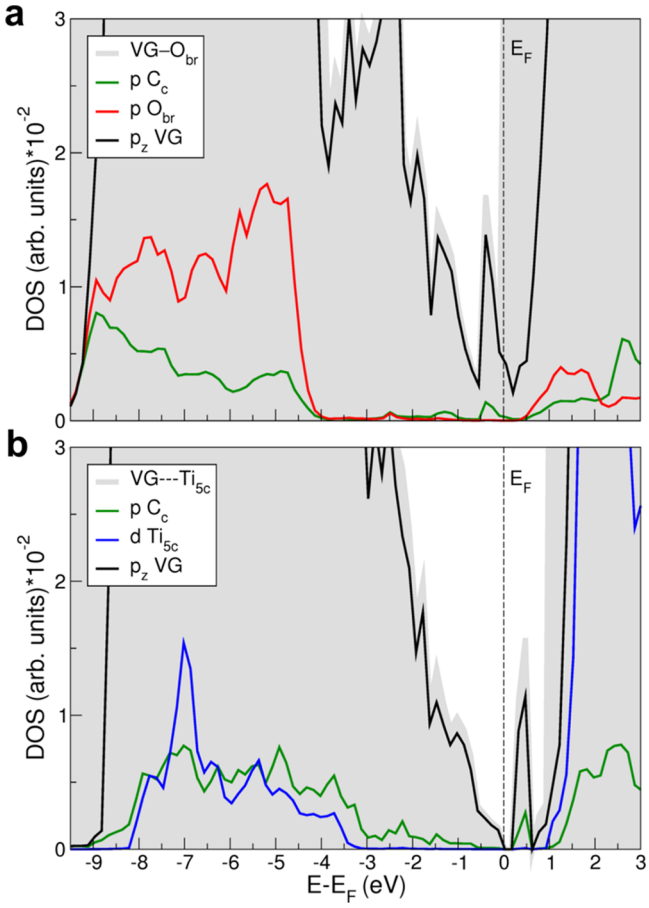

Figure 4. Total and projected DOS for the VG—O_{br} (a) and VG---Ti_{5c} (b) interfaces in a larger range of energies but in a zoomed range of density with respect to Figure 3. The green lines in (a) and (b) are DOS-projected on the p states of the C atom c marked in Figures 1 and 2. The red line in (a) is DOS-projected on the p states of the O_{br} atom on the TiO_2 surface bonding to the C atom c at the interface VG—O_{br}. The blue line in (b) is DOS-projected on the d states of the Ti_{5c} atom interacting with the C atom c at the interface VG---Ti_{5c}. The black lines in (a) and (b) are DOS-projected on the p_z states of all C atoms in VG. See Figures 2 and 3 for structures. Fermi energy (E_F) is set at the eigenvalue of the highest occupied states.

in the graphene sheet, in the confined zone between the two materials. Then, we evaluate the cover effect on the energetics of water dissociation on TiO_2(101) surface (Section 3.2.3). Finally, we investigate the electronic properties of hydrated VG/TiO_2 (Section 3.2.4) and the effect of an underlying reduced TiO_2 surface (Section 3.2.5).

3.2.1. Molecular Adsorption. We compare energy of adsorption (ΔE_{ads}), as defined in detail in Section 2. By comparing the systems in the top panel of Figure 5, it is evident that water binds more strongly on a 5-fold coordinated titanium (Ti_{5c}) of the anatase (101) TiO_2 surface (−0.97 eV) than on a defective graphene sheet (−0.22 eV), where it just weekly physisorbs by pointing the H atoms down toward the π electron density of the C layer.

As a next step, in the central panel of Figure 5, we consider that water comes from the top side of the two most stable interface configurations (see Figure 2). The adsorption energy (ΔE_{ads}) slightly increases with respect to the freestanding case by about −0.1 eV, which is probably due to some surface polarization induced by the presence of the titania substrate

DOI: 10.1021/acsami.7b18087
ACS Appl. Mater. Interfaces 2018, 10, 5793−5804

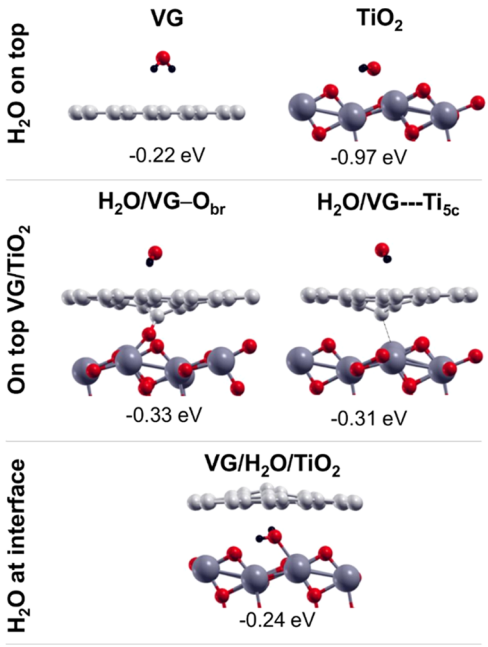

Figure 5. Side views of molecular water adsorption on top of freestanding VG and TiO_2(101) surface (top line), side views of molecular water adsorption on top of the most stable two VG/TiO_2 interfaces (middle line), and molecular water adsorption at the VG/TiO_2 interface (bottom line). Labels and adsorption energies are reported above and below each configuration, respectively, and defined in Section 2. Small red, light gray, and black balls represent O atoms, C atoms, and H atoms, respectively. Big dark gray balls represent Ti atoms.

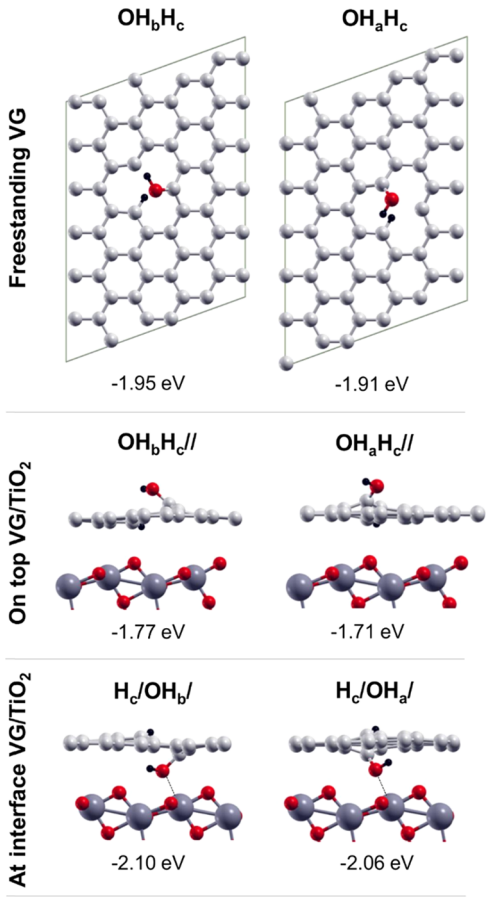

Figure 6. Top views of the partially dissociated products of water (OH + H) on freestanding VG (top line), side views of the partially dissociated products of water on top of VG/TiO_2 (middle line), and at the interfaces of VG/TiO_2 (bottom line). Labels and dissociation energies are reported above and below each configuration, respectively, and defined in Section 2. Small red, light gray, and black balls represent O atoms, C atoms, and H atoms. Big dark gray balls represent Ti atoms.

that enhanced the weak van der Waals interaction between the defective graphene sheet and the water molecule.

Finally, we have the water at the interface between the two materials, binding to a Ti_{5c} and with the two H atoms pointing toward the π electron density of the graphene sheet. However, the adsorption energy in this configuration is much smaller than on the top of TiO_2 surface (−0.24 vs −0.97 eV). The reason is that the graphene sheet must largely distort upward to give enough space to the water molecule, which accounts for a relevant energy cost. Moreover, the C sheet uplift highly reduces the adhesion energy between the two surfaces, which is a second relevant energy cost. The net balance (ΔE_{ads}) is still negative and comparable with water adsorption on top of VG/TiO_2 (−0.31/−0.33 eV).

3.2.2. Dissociated Adsorption. Water dissociation is typically in two fragments: OH and H. On a freestanding graphene sheet, as shown in the top panel of Figure 6, the OH fragment covalently binds to an under coordinated C atom of the vacancy, whereas the H atom covalently binds to another one. We have investigated more possibilities, among which the two lowest in energy are those shown in Figure 6: one with the OH on the C_b atom and the H on the C_c atom (OH_bH_c) and the other with the OH on the C_a and the H on the C_c (OH_aH_c). The dissociation energy values (ΔE_{diss}) are very similar and amount to about −1.9 eV. The dissociation energy becomes slightly smaller (by about 0.15−0.2 eV) when these types of dissociation happen on a TiO_2-supported graphene sheet, as a consequence of a reduced adhesion energy between the two materials due to the additional distortions. On the contrary, it becomes larger when the dissociation takes place at the interface (up to −2.10 eV). This is because the OH fragment establishes an additional stable bond with the Ti_{5c} on the anatase surface.

However, the OH + H dissociation mode is not the most favorable one on a defective graphene sheet. Further dissociation in O + H + H, or full dissociation, is found to produce a large energy gain. We considered many possible configurations; the four most stable ones are shown in Figure 7, whereas others are reported in the SI (see Figure S7). The two H atoms may either covalently bind to two different undercoordinated C atoms in graphene with the O atom forming a keto group on the third one ($O_aH_bH_c$ and $O_bH_aH_c$) or both bind to the same C atom (forming a CH_2 species), with the O atom forming an ether group with the other two undercoordinated C atoms (−COC− species) ($O_{ab}2H_c$ and $O_{bc}2H_a$). The most favored ones are the latter two with the $O_{ab}2H_c$ having the largest dissociation energy (ΔE_{diss}) of −4.37 eV.

When these dissociation processes happen on a supported graphene sheet, the energy gain is slightly less negative but the $O_{ab}2H_c$// configuration is still the most favorable (−4.32 eV). On the contrary, when these dissociations take place at the interface, we observed that the O of the keto group for the first two systems on the left side is largely stabilized by a strong

DOI: 10.1021/acsami.7b18087
ACS Appl. Mater. Interfaces 2018, 10, 5793−5804

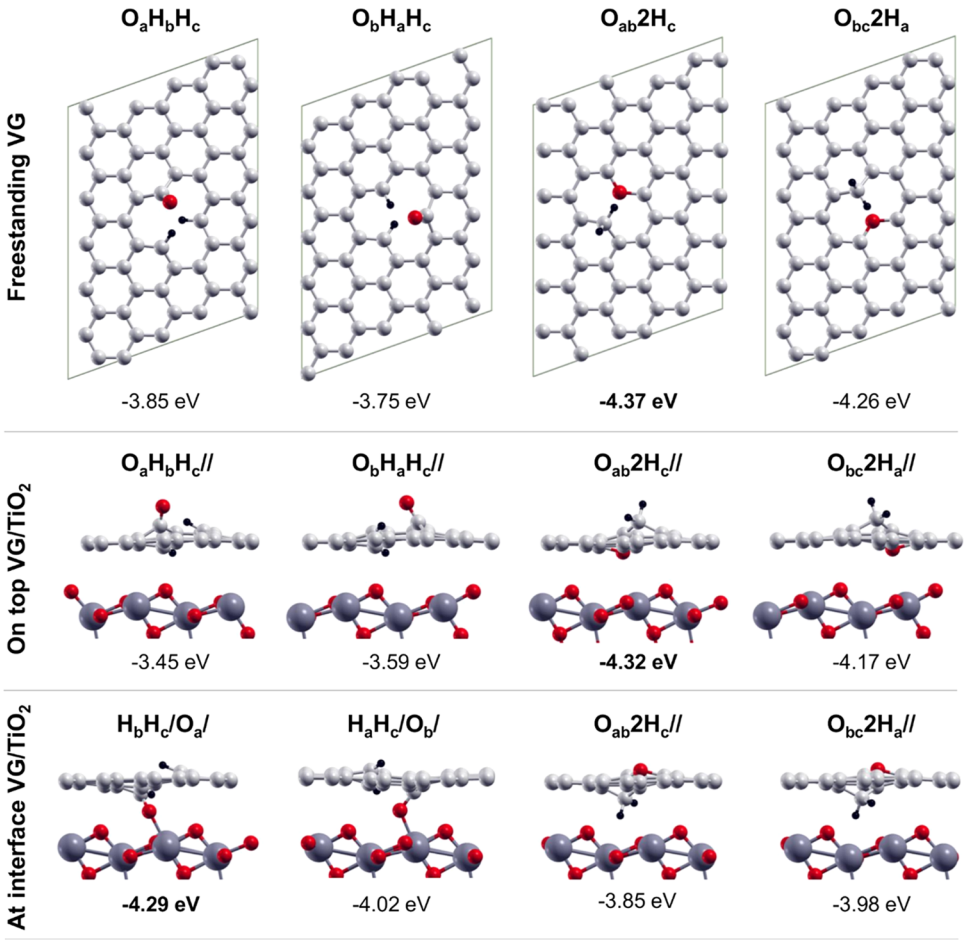

Figure 7. Top views of the fully dissociated products of water on freestanding VG (top line); side views of the fully dissociated products of water (O + H + H) on top of VG/TiO_2 (middle line), and at the interfaces of VG/TiO_2 (bottom line). Labels and dissociation energies are reported above and below each configuration, respectively, and defined in Section 2. Small red, light gray, and black balls represent O atoms, C atoms, and H atoms. Big dark gray balls represent Ti atoms.

interaction with the Ti_{5c} on the anatase surface. Therefore, an inversion in the relative stability is clearly observed and water dissociation at the VG/TiO_2 interface in the $H_bH_c/O_a/$ configuration becomes very stable with a ΔE_{diss} of −4.29 eV, similar to that of $O_{ab}2H_c//$.

In Figure 8, we show a number of configurations where either one or two H atoms are transferred to the TiO_2 surface. In one case, we even form an H_2 molecule that is physisorbed on the surface. However, as it is evident from analyzing the energies of dissociation, all of these configurations are less stable than those proposed in Figure 7, where both the H atoms saturated two undercoordinated C atoms of the defective graphene layer. Note that if one H atom is transferred, the O atom coming from the water saturates two C atoms by forming an ether group, whereas when both H atoms are transferred, the remaining O atoms replace the missing carbon in the graphene sheets and are 3-fold coordinated to the three undercoordinated C atoms of the vacancy (O_{abc}).

In the last part of this section devoted to water dissociation on and at the interface of VG/TiO_2, we are going to present an overview, as sketched in Figure 9, on what can actually happen when water comes from the top or is intercalated in the confined zone between the two materials, considering all of the configurations discussed above.

If water comes from the top, it may first physisorb ($H_2O//$) and then dissociate into two fragments ($OH_bH_c//$) and then further into three ($O_{ab}2H_c//$ or $O_{ab}H_bH_c//$). The final product $O_{ab}2H_c//$ is very stable (ΔE_{diss} = −4.32 eV) and more stable than $O_{ab}H_bH_c//$; however, the latter could eventually further evolve into the product $H_bH_c/O_a/$, where the O atom coming from the water full dissociation is bridging between a C atom of the graphene sheet and a Ti_{5c} atom on the TiO_2 surface. This final product is also extremely stable (ΔE_{diss} = −4.29 eV) and competes with $O_{ab}2H_c//$.

If water successfully intercalates in the interface zone, molecularly bound to a Ti_{5c} atom of the TiO_2 surface, there are several possibilities for the next chemical step: the water dissociation into two fragments (OH + H) may result in (i) an OH that is bridging between the two materials and the H bound to an undercoordinated C atom on graphene ($H_c/OH_a/$ and $H_c/OH_b/$), (ii) an OH that is bridging between the two materials and the H bound to the same C atom as the OH (H_c/OH_c), or (iii) into an OH that is bridging between the two materials and the H bound to a 2-fold O atom on the TiO_2 surface ($/OH_c/O_{br}H$). Each of these four (OH + H) configurations can evolve in a fully dissociated product (O + H + H), as described in Figure 9. The most stable final configuration is again the $H_bH_c/O_a/$, which was already discussed above (−4.29 eV). We wish to note that the OH

DOI: 10.1021/acsami.7b18087
ACS Appl. Mater. Interfaces 2018, 10, 5793−5804

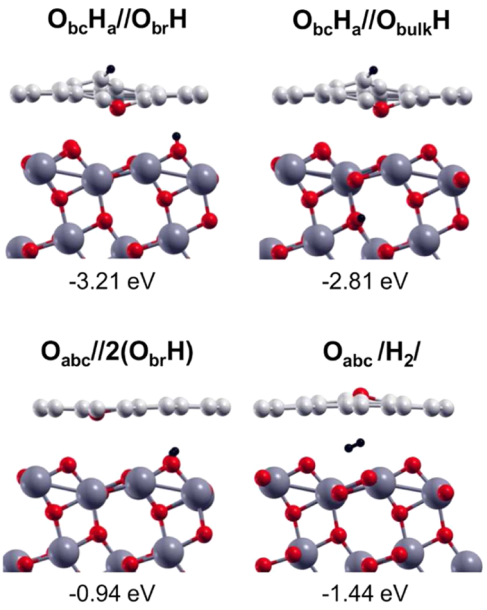

Figure 8. Side view of the total dissociation of water (O + H + H) with one H atom transferred to the O_{br} of the TiO_2 surface (top line, left) and the consequent diffusion of the H in the subsurface layer (top line, right). Side view of the total dissociation of water (O + H + H) with both H transferred to O_{br} atoms of the TiO_2 surface (bottom line, left), and finally, side view of the desorption of a H_2 molecule at the VG/TiO_2 interface (bottom line, right). Labels and dissociation energies are reported above and below each configuration, respectively, and defined in Section 2. Small red, light gray, and black balls represent O atoms, C atoms, and H atoms. Big dark gray balls represent Ti atoms.

species in the $H_c/OH_b/$ configuration is found to preferentially evolve into $H_aH_c/O_b/$ than into $H_c/O_b/O_{br}H$: −4.02 vs −2.09 eV.

Therefore, this analysis allows us to conclude that one of the most stable products, independently of the water origin, from the top or through the interface, is $H_bH_c/O_a/$, where there is an O atom strongly linked to both the materials: to graphene with a C−O covalent bond (1.26 Å) and to TiO_2 with a Ti−O strong covalent bond (2.06 Å).

3.2.3. Cover Effect. In this last section, we analyze the cover effect on water dissociation. Although the cover effect on molecular water adsorption on TiO_2 is a negative one (from −0.97 to −0.24 eV), as shown in Figure 5 and discussed in Section 3.2.1, in the case of dissociated water, the cover effect is positive and largely stabilizes the OH + H dissociation (from −0.63 to −1.02 eV) by forming a bridging species with the OH bound to both a C atom of the graphene sheet and a Ti atom on the TiO_2 surface (see Figure 10).

3.2.4. Electronic Properties of Hydrated VG/TiO_2. We investigated the electronic properties of the two most stable structures resulting from full dissociation of water on VG/TiO_2, which are $O_{ab}2H_c//$ and $H_bH_c/O_a/$. The aim is to determine the water effect on the electronic properties of the composite. We recall from Section 3.1 that VG—O_{br} is metallic, whereas VG---Ti_{5c} is semiconducting with a 0.27 eV band gap (see DOS in Figure 3). After water dissociation, we observe a semiconducting character in the DOS (Figure S8 in SI) of both the hydrated structures ($O_{ab}2H_c//$ and $H_bH_c/O_a/$) with a band gap of 0.49 and 0.40 eV, respectively.

3.2.5. Effect of an Underlying Reduced TiO_2 Surface. In this last section, we discuss what could happen if the TiO_2 system were reduced, as often is the case in real samples. We thus considered the possibility that the full dissociation of water (configuration $H_bH_c/O_a/$) takes place on a nonstoichiometric TiO_2 slab, presenting an oxygen vacancy V_O in the second layer of the slab ($H_bH_c/O_a/V_O$), as shown on the left side of Figure 11. Considering that excess O atoms on the surface are known to diffuse into the bulk of TiO_2 to heal eventual subsurface or bulk oxygen vacancies in anatase TiO_2,[73] we transferred the O atom from the interface to the V_O site and fully relaxed the structure ($H_bH_c//$), as shown on the right side of Figure 11. The energy gain that is computed is rather large because it amounts to −1.76 eV. Therefore, we may conclude that the presence of an underlying reduced metal oxide support may further complete the water splitting at the VG/TiO_2 interface by attracting the oxygen atom from water into the subsurface layers or in the bulk of the oxide where vacancies are present.

4. CONCLUSIONS

In summary, the atomic structure of the interface between defective graphene and anatase TiO_2 surface, together with its electronic properties and chemical reactivity with water molecules, were systematically investigated by dispersion-corrected hybrid density functional calculations. The magnetism observed for the carbon monovacancy model in graphene (VG) is found to quench when VG is put on TiO_2(101) surface. The interaction at the VG/TiO_2 interface is typically based on van der Waals or dispersion forces. However, after overcoming some energy barrier, a C−O bond may be formed at the interface. The chemical adsorption of VG on TiO_2(101) leads to a metallic character of the hybrid system, whereas the physical adsorption presents semiconducting properties, with a small band gap of 0.27 eV. The adsorption energy of molecular water on top of VG/TiO_2 interface is slightly increased with respect to the freestanding case by about −0.1 eV. Water molecules can dissociate either on top or at the VG/TiO_2 interface. Our study allowed the definition of the possible reaction paths and of the most stable dissociation products. Full dissociation into O + H + H is found to be largely preferred. These configurations involve the formation of a methylene (CH_2) and one ether (−COC−) group at the C vacancy site in VG ($O_{ab}2H_c//$) or two CH bonds and the O atom strongly linked to both materials, forming a C−O bond on one side and a O−Ti_{5c} bond on the other ($H_bH_c/O_a/$). This O atom is an interface species. Very importantly, if the underlying TiO_2 substrate is partially reduced, with oxygen vacancies in the subsurface layers, this interface O atom is found to be subject to a force that would favorably drive it down to heal the vacancy (by −1.8 eV). Then, water splitting is fully achieved because the two H atoms are left on the graphene layer, whereas the O atom is deep in the TiO_2 bulk.

To conclude, this comprehensive study provides important information on the details of the atomic structure and electronic properties of graphene/titania composites, even when the conditions are not as ideal as one would wish, i.e., in the presence of C vacancies in the graphene sheet prepared on top of the TiO_2 sample, in the presence of unwanted water molecules in the experimental conditions, and in the presence of oxygen vacancies when the TiO_2 sample is not fully stoichiometric because of reducing preparation conditions or because of severe annealing processes. The results give a clear overview of what chemistry would take place in these real complex composite systems.

DOI: 10.1021/acsami.7b18087
ACS Appl. Mater. Interfaces 2018, 10, 5793−5804

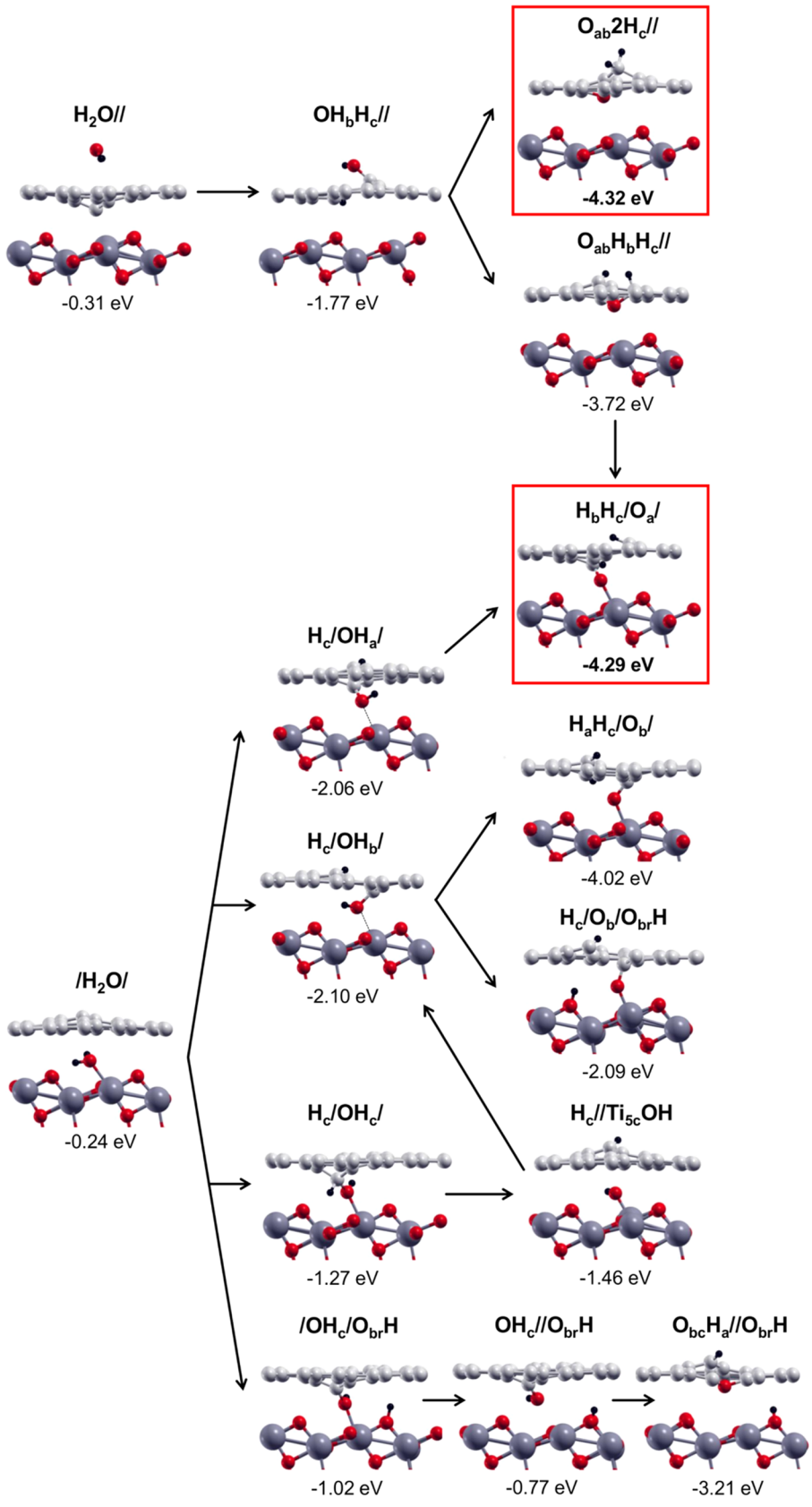

Figure 9. Side views of water adsorption on top or at the VG/TiO_2 interface (left column); side views of partial water dissociation in OH and H on top and at the VG/TiO_2 interfaces (middle column), and finally side views of the various possible steps of total water dissociation (right column). Labels and adsorption/dissociation energies are reported above and below each configuration, respectively, and defined in Section 2. Small red, light gray, and black balls represent O atoms, C atoms, and H atoms. Big dark gray balls represent Ti atoms.

DOI: 10.1021/acsami.7b18087
ACS Appl. Mater. Interfaces 2018, 10, 5793−5804

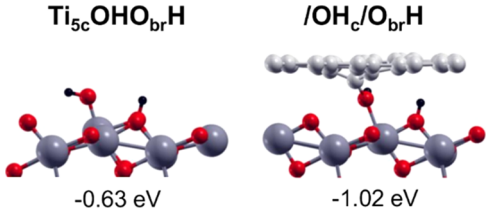

Figure 10. On the left side, view of water dissociation on bare TiO_2(101) surface and on the right, the cover effect of defective graphene on water dissociation at TiO_2 surface. Labels and dissociation energies are reported above and below each configuration, respectively, and defined in Section 2. Small red, light gray, and black balls represent O atoms, C atoms, and H atoms. Big dark gray balls represent Ti atoms.

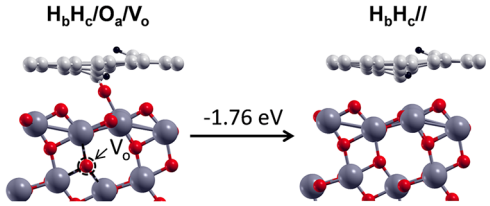

Figure 11. On the left, side view of the fully dissociated product of water at the VG/TiO_2 interface, with one oxygen vacancy (V_O) in the subsurface layer of TiO_2. On the right, the oxygen O_a from the water heals the V_O in TiO_2. The energy gain during the transfer/healing process is shown on top of the arrow. Labels are reported above each configuration. Small red, light gray, and black balls represent O atoms, C atoms, and H atoms. Big dark gray balls represent Ti atoms. The dotted black circle represents the V_O in TiO_2.

■ ASSOCIATED CONTENT

Supporting Information

The Supporting Information is available free of charge on the ACS Publications website at DOI: 10.1021/acsami.7b18087.

Top views of vacancy patterns in VG_{ab} and VG_{bc} due to the repetition of the supercell; side views of configurations of VG_{bc}/TiO_2 interfaces in the singlet close shell and triplet solutions; side views of configurations of VG_{ab}/TiO_2 interfaces in the singlet close shell and triplet solutions; total and projected DOS for the physical adsorption of water on freestanding graphene with and without vacancy; four HOMO and two LUMO of isolated water molecule (upper part), charge density of four highest occupied bands and two lowest unoccupied bands for H_2O/G and H_2O/VG_{ab}; top and side views of the partially and fully dissociated products of water on freestanding VG; top views of the fully dissociated products of water on freestanding VG, side views of the fully dissociated products of water on top of the interface VG/TiO_2, and at the interface VG/TiO_2; total and projected DOS for $O_{ab}2H_c$// and H_bH_c/O_a/ (PDF)

■ AUTHOR INFORMATION

Corresponding Author

*E-mail: cristiana.divalentin@unimib.it.

ORCID

Cristiana Di Valentin: 0000-0003-4163-8062

Notes

The authors declare no competing financial interest.

■ ACKNOWLEDGMENTS

The authors are grateful to Lorenzo Ferraro for his technical help. The project has received funding from the European Research Council (ERC) under the European Union's HORIZON2020 research and innovation program (ERC Grant Agreement No. 647020).

■ REFERENCES

(1) Novoselov, K. S.; Geim, A. K.; Morozov, S. V.; Jiang, D.; Zhang, Y.; Dubonos, S. V.; Grigorieva, I. V.; Firsov, A. A. Electric Field Effect in Atomically Thin Carbon Films. *Science* **2004**, *306*, 666−669.

(2) Geim, A. K.; Novoselov, K. S. The Rise of Graphene. *Nat. Mater.* **2007**, *6*, 183−191.

(3) Castro Neto, A. H.; Guinea, F.; Peres, N. M. R.; Novoselov, K. S.; Geim, A. K. The Electronic Properties of Graphene. *Rev. Mod. Phys.* **2009**, *81*, 109−162.

(4) Deng, D.; Novoselov, K. S.; Fu, Q.; Zheng, N.; Tian, Z.; Bao, X. Catalysis with Two-dimensional Materials and Their Heterostructures. *Nat. Nanotechnol.* **2016**, *11*, 218−230.

(5) Yao, Y.; Fu, Q.; Zhang, Y. Y.; Weng, X.; Li, H.; Chen, M.; Jin, L.; Dong, A.; Mu, R.; Jiang, P.; Liu, L.; Bluhm, H.; Liu, Z.; Zhang, S. B.; Bao, X. Graphene Cover-promoted Metal-catalyzed Reactions. *Proc. Natl. Acad. Sci. U.S.A.* **2014**, *111*, 17023−17028.

(6) Deng, J.; Deng, D.; Bao, X. Robust Catalysis on 2D Materials Encapsulating Metals: Concept, Application, and Perspective. *Adv. Mater.* **2017**, *29*, No. 1606967.

(7) Han, L.; Wang, P.; Dong, S. Progress in Graphene-based Photoactive Nanocomposites as a Promising Class of Photocatalyst. *Nanoscale* **2012**, *4*, 5814.

(8) Xiang, Q.; Yu, J.; Jaroniec, M. Graphene-based Semiconductor Photocatalysts. *Chem. Soc. Rev.* **2012**, *41*, 782−796.

(9) Yang, M.-Q.; Zhang, N.; Pagliaro, M.; Xu, Y.-J. Artificial Photosynthesis over Graphene-semiconductor Composites. Are We Getting Better? *Chem. Soc. Rev.* **2014**, *43*, 8240−8254.

(10) Roy-Mayhew, J. D.; Aksay, I. A. Graphene Materials and Their Use in Dye-sensitized Solar Cells. *Chem. Rev.* **2014**, *114*, 6323−6348.

(11) Lee, J. S.; You, K. H.; Park, C. B. Highly Photoactive, Low Band Gap TiO_2 Nanoparticles Wrapped by Graphene. *Adv. Mater.* **2012**, *24*, 1084−1088.

(12) Liu, H.; Lv, T.; Zhu, Z. Template-assisted Synthesis of Hollow TiO_2@rGO Core−shell Structural Nanospheres with Enhanced Photocatalytic Activity. *J. Mol. Catal. A: Chem.* **2015**, *404*−*405*, 178−185.

(13) Xu, C.; Zhu, J.; Yuan, R.; Fu, X. More Effective Use of Graphene in Photocatalysis by Conformal Attachment of Small Sheets to TiO_2 Spheres. *Carbon* **2016**, *96*, 394−402.

(14) Liu, H.; Liu, S.; Zhang, Z.; Dong, X.; Liu, T. Hydrothermal Etching Fabrication of TiO_2@graphene Hollow Structures: Mutually Independent Exposed {001} and {101} Facets Nanocrystals and Its Synergistic Photocaltalytic Effects. *Sci. Rep.* **2016**, *6*, No. 33839.

(15) Huang, Q.; Tian, S.; Zeng, D.; Wang, X.; Song, W.; Li, Y.; Xiao, W.; Xie, C. Enhanced Photocatalytic Activity of Chemically Bonded TiO_2/Graphene Composites Based on the Effective Interfacial Charge Transfer through the C−Ti Bond. *ACS Catal.* **2013**, *3*, 1477−1485.

(16) Low, J.; Yu, J.; Ho, W. Graphene-Based Photocatalysts for CO_2 Reduction to Solar Fuel. *J. Phys. Chem. Lett.* **2015**, *6*, 4244−4251.

(17) Tan, L. L.; Chai, S. P.; Mohamed, A. R. Synthesis and Applications of Graphene-based TiO_2 Photocatalysts. *ChemSusChem* **2012**, *5*, 1868−1882.

(18) Zhou, K.; Zhu, Y.; Yang, X.; Jiang, X.; Li, C. Preparation of Graphene−TiO_2 Composites with Enhanced Photocatalytic Activity. *New J. Chem.* **2011**, *35*, 353−359.

(19) Ferrighi, L.; Fazio, G.; Di Valentin, C. Charge Carriers Separation at the Graphene/(101) Anatase TiO_2 Interface. *Adv. Mater. Interfaces* **2016**, *3*, No. 1500624.

(20) Williams, K. J.; Nelson, C. A.; Yan, X.; Li, L.-S.; Zhu, X. Hot Electron Injection from Graphene Quantum Dots to TiO_2. *ACS Nano* **2013**, *7*, 1388−1394.

DOI: 10.1021/acsami.7b18087
ACS Appl. Mater. Interfaces 2018, 10, 5793−5804

(21) Bachmatiuk, A.; Mendes, R. G.; Hirsch, C.; Jähne, C.; Lohe, M. R.; Grothe, J.; Kaskel, S.; Fu, L.; Klingeler, R.; Eckert, J.; Wick, P.; Rümmeli, M. H. Few-Layer Graphene Shells and Nonmagnetic Encapsulates: A Versatile and Nontoxic Carbon Nanomaterial. *ACS Nano* **2013**, *7*, 10552−10562.
(22) Wu, R.; Shen, S.; Xia, G.; Zhu, F.; Lastoskie, C.; Zhang, J. Soft-Templated Self-Assembly of Mesoporous Anatase TiO_2/Carbon Composite Nanospheres for High-Performance Lithium Ion Batteries. *ACS Appl. Mater. Interfaces* **2016**, *8*, 19968−19978.
(23) Tong, X.; Zeng, M.; Li, J.; Li, F. UV-assisted Synthesis of Surface Modified Mesoporous TiO_2/G Microspheres and Its Electro Chemical Performances in Lithium Ion Batteries. *Appl. Surf. Sci.* **2017**, *392*, 897−903.
(24) Liu, H.; Guo, K.; Duan, C.; Dong, X.; Gao, J. Hollow TiO_2 Modified Reduced Graphene Oxide Microspheres Encapsulating Hemoglobin for a Mediator-free Biosensor. *Biosens. Bioelectron.* **2017**, *87*, 473−479.
(25) Zhao, H.; Ding, R.; Zhao, X.; Li, Y.; Qu, L.; Pei, H.; Yildirimer, L.; Wu, Z.; Zhang, W. Graphene-based Nanomaterials for Drug and/or Gene Delivery, Bioimaging, and Tissue Engineering. *Drug Discovery Today* **2017**, *22*, 1302−1317.
(26) Rajh, T.; Dimitrijevic, N. M.; Bissonnette, M.; Koritarov, T.; Konda, V. Titanium Dioxide in the Service of the Biomedical Revolution. *Chem. Rev.* **2014**, *114*, 10177−10216.
(27) Banhart, F.; Kotakoski, J.; Krasheninnikov, A. V. Structural Defects in Graphene. *ACS Nano* **2011**, *5*, 26−41.
(28) Terrones, H.; Lv, R.; Terrones, M.; Dresselhaus, M. S. The Role of Defects and Doping in 2D Graphene Sheets and 1D Nanoribbons. *Rep. Prog. Phys.* **2012**, *75*, No. 062501.
(29) Zhang, N.; Yang, M.; Liu, S.; Sun, Y.; Xu, Y. Waltzing with the Versatile Platform of Graphene to Synthesize Composite Photocatalysts. *Chem. Rev.* **2015**, *115*, 10307−10377.
(30) Liang, Y. T.; Vijayan, B. K.; Gray, K. A.; Hersam, M. C. Minimizing Graphene Defects Enhances Titania Nanocomposite-Based Photocatalytic Reduction of CO_2 for Improved Solar Fuel Production. *Nano Lett.* **2011**, *11*, 2865−2870.
(31) Zhang, Y.; Zhang, N.; Tang, Z.; Xu, Y. Improving the Photocatalytic Performance of Graphene−TiO_2 Nanocomposites via a Combined Strategy of Decreasing Defects of Graphene and Increasing Interfacial Contact. *Phys. Chem. Chem. Phys.* **2012**, *14*, 9167−9175.
(32) Gass, M. H.; Bangert, U.; Bleloch, A. L.; Wang, P.; Nair, R. R.; Geim, A. K. Free-standing Graphene at Atomic Resolution. *Nat. Nanotechnol.* **2008**, *3*, 676−681.
(33) Meyer, J. C.; Kisielowski, C.; Erni, R.; Rossell, M. D.; Crommie, M. F.; Zettl, A. Direct Imaging of Lattice Atoms and Topological Defects in Graphene Membranes. *Nano Lett.* **2008**, *8*, 3582−3586.
(34) Rodríguez-Manzo, J. A.; Cretu, O.; Banhart, F. Trapping of Metal Atoms in Vacancies of Carbon Nanotubes and Graphene. *ACS Nano* **2010**, *4*, 3422−3428.
(35) Zoberbier, T.; Chamberlain, T. W.; Biskupek, J.; Suyetin, M.; Majouga, A. G.; Besley, E.; Kaiser, U.; Khlobystov, A. N. Investigation of the Interactions and Bonding between Carbon and Group VIII Metals at the Atomic Scale. *Small* **2016**, *12*, 1649−1657.
(36) Fampiou, I.; Ramasubramaniam, A. Influence of Support Effects on CO Oxidation Kinetics on CO-Saturated Graphene-Supported Pt_{13} Nanoclusters. *J. Phys. Chem. C* **2015**, *119*, 8703−8710.
(37) Lim, D.-H.; Wilcox, J. Mechanisms of the Oxygen Reduction Reaction on Defective Graphene-Supported Pt Nanoparticles from First-Principles. *J. Phys. Chem. C* **2012**, *116*, 3653−3660.
(38) Kim, K.; Lee, H. B.; Johnson, R. W.; Tanskanen, J. T.; Liu, N.; Kim, M. G.; Pang, C.; Ahn, C.; Bent, S. F.; Bao, Z. Selective Metal Deposition at Graphene Line Defects by Atomic Layer Deposition. *Nat. Commun.* **2014**, *5*, No. 4781.
(39) Kim, G.; Jhi, S. H.; Lim, S.; Park, N. Effect of Vacancy Defects in Graphene on Metal Anchoring and Hydrogen Adsorption. *Appl. Phys. Lett.* **2009**, *94*, No. 173102.
(40) Ramos-Castillo, C. M.; Reveles, J. U.; Zope, R. R.; de Coss, R. Palladium Clusters Supported on Graphene Monovacancies for Hydrogen Storage. *J. Phys. Chem. C* **2015**, *119*, 8402−8409.
(41) Junkaew, A.; Rungnim, C.; Kunaseth, M.; Arroyave, R.; Promarak, V.; Kungwan, N.; Namuangruk, S. Metal Cluster-deposited Graphene as an Adsorptive Material for m-xylene. *New J. Chem.* **2015**, *39*, 9650−9658.
(42) Ferrighi, L.; Perilli, D.; Selli, D.; Di Valentin, C. Water at the Interface Between Defective Graphene and Cu or Pt (111) Surfaces. *ACS Appl. Mater. Interfaces* **2017**, *9*, 29932−29941.
(43) Ferrighi, L.; Datteo, M.; Fazio, G.; Di Valentin, C. Enhanced Reactivity at the Interface between (Doped) Graphene and Anatase TiO_2. *J. Am. Chem. Soc.* **2016**, *138*, 7365−7376.
(44) Mu, R.; Fu, Q.; Jin, L.; Yu, L.; Fang, G.; Tan, D.; Bao, X. Visualizing Chemical Reactions Confined under Graphene. *Angew. Chem., Int. Ed.* **2012**, *51*, 4856−4859.
(45) Zhang, Y.; Fu, Q.; Cui, Y.; Mu, R.; Jin, L.; Bao, X. Enhanced Reactivity of Graphene Wrinkles and Their Function as Nanosized Gas Inlets for Reactions Under Graphene. *Phys. Chem. Chem. Phys.* **2013**, *15*, 19042−19048.
(46) Zhang, Y.; Weng, X.; Li, H.; Li, H.; Wei, M.; Xiao, J.; Liu, Z.; Chen, M.; Fu, Q.; Bao, X. Hexagonal Boron Nitride Cover on Pt(111): A New Route to Tune Molecule−Metal Interaction and Metal-Catalyzed Reactions. *Nano Lett.* **2015**, *15*, 3616−3623.
(47) Wei, M.; Fu, Q.; Wu, H.; Dong, A.; Bao, X. Hydrogen Intercalation of Graphene and Boron Nitride Monolayers Grown on Pt(111). *Top. Catal.* **2016**, *59*, 543−549.
(48) Kidambi, P. R.; Bayer, B. C.; Blume, R.; Wang, Z. J.; Baehtz, C.; Weatherup, R. S.; Willinger, M. G.; Schloegl, R.; Hofmann, S. Observing Graphene Grow: Catalyst-graphene Interactions During Scalable Graphene Growth on Polycrystalline Copper. *Nano Lett.* **2013**, *13*, 4769−4778.
(49) Reckinger, N.; Van Hooijdonk, E.; Joucken, F.; Tyurnina, A. V.; Lucas, S.; Colomer, J. F. Anomalous Moiré Pattern of Graphene Investigated by Scanning Tunneling Microscopy: Evidence of Graphene Growth on Oxidized Cu(111). *Nano Res.* **2014**, *7*, 154−162.
(50) Ferrighi, L.; Di Valentin, C. Oxygen Reactivity on Pure and B-doped Graphene over Crystalline Cu(111). Effects of the Dopant and of the Metal Support. *Surf. Sci.* **2015**, *634*, 68−75.
(51) Olson, E. J.; Ma, R.; Sun, T.; Ebrish, M. A.; Haratipour, N.; Min, K.; Aluru, N. R.; Koester, S. J. Capacitive Sensing of Intercalated H_2O Molecules Using Graphene. *ACS Appl. Mater. Interfaces* **2015**, *7*, 25804−25812.
(52) Lee, D.; Ahn, G.; Ryu, S. Two-dimensional Water Diffusion at a Graphene-silica Interface. *J. Am. Chem. Soc.* **2014**, *136*, 6634−6642.
(53) Lu, H.; Lipatov, A.; Ryu, S.; Kim, D. J.; Lee, H.; Zhuravlev, M. Y.; Eom, C. B.; Tsymbal, E. Y.; Sinitskii, A.; Gruverman, A. Ferroelectric Tunnel Junctions with Graphene Electrodes. *Nat. Commun.* **2014**, *5*, No. 5518.
(54) Politano, A.; Cattelan, M.; Boukhvalov, D. W.; Campi, D.; Cupolillo, A.; Agnoli, S.; Apostol, N. G.; Lacovig, P.; Lizzit, S.; Farías, D.; Chiarello, G.; Granozzi, G.; Larciprete, R. Unveiling the Mechanisms Leading to H_2 Production Promoted by Water Decomposition on Epitaxial Graphene at Room Temperature. *ACS Nano* **2016**, *10*, 4543−4549.
(55) Feng, X.; Maier, S.; Salmeron, M. Water Splits Epitaxial Graphene and Intercalates. *J. Am. Chem. Soc.* **2012**, *134*, 5662−5668.
(56) Boukhvalov, D. W.; Son, Y. W.; Ruoff, R. S. Water Splitting over Graphene-Based Catalysts: Ab Initio Calculations. *ACS Catal.* **2014**, *4*, 2016−2021.
(57) Böttcher, S.; Vita, H.; Weser, M.; Bisti, F.; Dedkov, Y. S.; Horn, K. Adsorption of Water and Ammonia on Graphene: Evidence for Chemisorption from X-ray Absorption Spectra. *J. Phys. Chem. Lett.* **2017**, *8*, 3668−3672.
(58) Voloshina, E.; Usvyat, D.; Schütz, M.; Dedkovcd, Y.; Paulusa, B. On the physisorption of water on graphene: a CCSD(T) study. *Phys. Chem. Chem. Phys.* **2011**, *13*, 12041−12047.

DOI: 10.1021/acsami.7b18087
ACS Appl. Mater. Interfaces 2018, 10, 5793−5804

(59) Böttcher, S.; Weser, M.; Dedkov, Y.; Horn, K.; Voloshina, E. N.; Paulus, B. Graphene on Ferromagnetic Surfaces and Its Functionalization with Water and Ammonia. *Nanoscale Res. Lett.* **2011**, *6*, 214.
(60) Ronchi, C.; Datteo, M.; Perilli, D.; Ferrighi, L.; Fazio, G.; Selli, D.; Di Valentin, C. π Magnetism of Carbon Monovacancy in Graphene by Hybrid Density Functional Calculations. *J. Phys. Chem. C* **2017**, *121*, 8653−8661.
(61) Dovesi, R.; Orlando, R.; Erba, A.; Zicovich-Wilson, C. M.; Civalleri, B.; Casassa, S.; Maschio, L.; Ferrabone, M.; Pierre, M. D. L.; D'Arco, P.; Noël, Y.; Causà, M.; Rérat, M.; Kirtman, B. CRYSTAL14: A Program for the Ab Initio Investigation of Crystalline Solids. *Int. J. Quantum Chem.* **2014**, *114*, 1287−1317.
(62) Lee, C.; Yang, W.; Parr, R. G. Development of the Colle-Salvetti Correlation-energy Formula into a Functional of the Electron Density. *Phys. Rev. B* **1988**, *37*, 785−789.
(63) Becke, A. D. Density-functional Thermochemistry. III. The Role of Exact Exchange. *J. Chem. Phys.* **1993**, *98*, 5648−5652.
(64) Grimme, S. Semiempirical GGA-type Density Functional Constructed with a Long-range Dispersion Correction. *J. Comput. Chem.* **2006**, *27*, 1787−1799.
(65) Civalleri, B.; Zicovich-Wilson, C. M.; Valenzano, L.; Ugliengo, P. B3LYP Augmented with an Empirical Dispersion Term (B3LYP-D*) as Applied to Molecular Crystals. *CrystEngComm* **2008**, *10*, 405−410.
(66) Liu, L.; Liu, Z.; Liu, A.; Gu, X.; Ge, C.; Gao, F.; Dong, L. Engineering the TiO_2−Graphene Interface to Enhance Photocatalytic H_2 Production. *ChemSusChem* **2014**, *7*, 618−626.
(67) Wang, P.; Zhan, S.; Xia, Y.; Ma, S.; Zhou, Q.; Li, Y. The Fundamental Role and Mechanism of Reduced Graphene Oxide in rGO/Pt-TiO_2 Nanocomposite for High-performance Photocatalytic Water Splitting. *Appl. Catal., B* **2017**, *207*, 335−346.
(68) Zhang, H.; Lv, X.; Li, Y.; Wang, Y.; Li, J. P25-Graphene Composite as a High Performance Photocatalyst. *ACS Nano* **2010**, *4*, 380−386.
(69) Vijayan, B. K.; Dimitrijevic, N. M.; Finkelstein-Shapiro, D.; Wu, J.; Gray, K. A. Coupling Titania Nanotubes and Carbon Nanotubes To Create Photocatalytic Nanocomposites. *ACS Catal.* **2012**, *2*, 223−229.
(70) Ayissi, S.; Charpentier, P. A.; Farhangi, N.; Wood, J. A.; Palotás, K.; Hofer, W. A. Interaction of Titanium Oxide Nanostructures with Graphene and Functionalized Graphene Nanoribbons: A DFT Study. *J. Phys. Chem. C* **2013**, *117*, 25424−25432.
(71) Bukowski, B.; Deskins, N. A. The Interactions between TiO_2 and Graphene with Surface Inhomogeneity Determined Using Density Functional Theory. *Phys. Chem. Chem. Phys.* **2015**, *17*, 29734−29746.
(72) Xiang, Q.; Yu, J.; Jaroniec, M. Enhanced Photocatalytic H_2-production Activity of Graphene-modified Titania Nanosheets. *Nanoscale* **2011**, *3*, 3670.
(73) Setvín, M.; Aschauer, U.; Scheiber, P.; Li, Y.; Hou, W.; Schmid, M.; Selloni, A.; Diebold, U. Reaction of O_2 with Subsurface Oxygen Vacancies on TiO_2 Anatase (101). *Science* **2013**, *341*, 988−991.

DOI: 10.1021/acsami.7b18087
ACS Appl. Mater. Interfaces 2018, 10, 5793−5804